SICEL VII Simposio Internacional sobre Calidad de la Energía Eléctrica 2013

Two Degrees of Freedom Control add Repetitive Controller for Inverters Working in Island Mode in Microgrids

R. Ortega[1], O. Carranza[1], jcsosa@ipn.mx[1], C.L. Trujillo[2]
[1]Escuela Superior de Cómputo, Instituto Politécnico Nacional, México D.F., e-mail: rortegag@ipn.mx, ocarranzac@ipn.mx. [2]Departamento de Ingeniería Electrónica, Universidad Distrital Francisco José de Caldas. Carrera 7 Nº 40-53 Piso 5, Bogotá, Colombia, e-mail: cltrujillo@udistrital.edu.co

Abstract. **This paper presents the analysis and design of an innovative control scheme that significantly reduces the Voltage Total Harmonic Distortion (THDv) of power inverters connected to microgrids working in island mode. The proposed Repetitive Two-Degrees of Freedom (R2DOF) control scheme combines the advantages of both repetitive and two-degrees of freedom control techniques, both controllers reduce the THDv in the presence of nonlinear loads. As it is shown in the paper, the inverter performance is improved by the proposed concept even when strongly nonlinear loads are connected to the microgrid. The analysis and design of the whole control system is presented in detail.**

Key words: Two degrees of freedom control, Repetitive controller, Inverter, Microgrids.

I. Introduction

TODAY as a result of increased electricity demand, governments are promoting new and cleaner power generation sources, the so-called renewable energies, such as solar, wind, and fuel cells among others. Under this new scheme of electricity generation it is necessary to use interfaces capable of transferring energy from renewable sources to the power grid, as well to feed loads when the power grid is absent. Microgrids are able of working in both previously described operation modes: grid connection mode and isolated mode. Usually, microgrids are composed by low and medium voltage systems fed from distributed generation sources such as microturbines, fuel cells or photovoltaic systems together with energy storage devices and loads [1-2]. These systems allow that the energy generation is near to consumption points, leading to the Distributed Generation (DG) scenario.

A microgrid is able to import and export energy in a flexible manner on the grid, controlling the flow of active power and reactive power, as well as managing energy storage. The inverters working in a microgrid have the ability to operate both in island mode and in grid connected mode. The inverters can be parallelized to handle more loads. It is important that the inverter imposes an appropriate voltage waveform operating in island mode [3]. The voltage must comply with amplitude and frequency conditions; regardless of the type of load is connected. Additionally, an adequate THDv, less than 5% according to the standar IEEE 519-1992 [4], should be ensured. In order to achieve this goal, repetitive [5] and two degrees of freedom (2DOF) control [6] have been proposed in the past. Both controllers reduce the THDv in the presence of nonlinear loads. The current harmonics produced by nonlinear loads generate distortion in the voltage waveform, resonance and noise in the system [7].

In this paper the combination of repetitive and 2DOF control is proposed for the control of microgrid inverters working in island mode, showing the resulting advantages. The paper is organized as follows. First, the systems description will be presented. Second, the inverter circuit will be modeled in order to obtain the transfer functions needed to design the control loops. Third, inverter controllers in island mode will be designed. Fourth, the controllers will be validated by both PSIM™ [8] simulations and experimental results. Finally, some conclusions will be drawn.

II. System Description

Fig.1 shows an H-bridge inverter operating in island mode. The inverter is fed by a photovoltaic panels array followed by a DC-DC converter, which provides a regulated DC input voltage to the inverter, VDC=400Vdc, when the inverter is operating in island mode. The inverter output voltage is $230V_{rms}$ and 50Hz. Sinusoidal bipolar PWM modulation has been chosen for the inverter because it reduces the common mode currents (CMC) injected to the load [9].

Table 1 shows the inverter main parameters. For the design of the controllers it is necessary to identify the transfer functions of the variables to control. The transfer functions are extracted using the technique of PWM switch modeling [10]. The mathematical models that allow obtaining the transfer functions of interest for the control are presented in the next section.

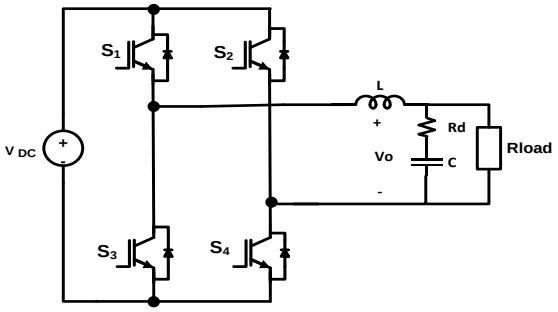

Fig.1. Schematic of the inverter in island mode operation.

TABLE I
PARAMETERS OF THE INVERTER UNDER STUDY

Parameter	Values
Nominal active power (P)	440 W
DC Link voltage (V_{DC})	400V
Inverter output voltage (VO)	230VRMS
Inverter output frequency (f_g)	50Hz
Inverter inductance (L)	19 mH
Inverter output capacitor (C)	600 nF
Damping resistance (R_d)	5Ω
Inverter switching frequency (fsi)	20 kHz
Load resistance (R_{LOAD}) at full power	120 Ω

III. SMALL SIGNAL MODEL

In this section the inverter circuit is averaged and perturbed around its operation point in order to obtain a linear small-signal model. The inverter load under consideration is resistive.

The inverter dynamics is similar to that of a Buck circuit [11], taking into account that in the inverter the operation point (D, Vo, I_L) varies periodically at 50Hz, as it will be shown further.

Equation (1) shows the relationship between the averaged inverter output voltage, v_o, and the input voltage, v_{DC}, in terms of the averaged duty cycle d. The average of each variable is calculated in each cycle of the switching frequency.

$$v_o = v_{DC} \cdot (2 \cdot d - 1) \tag{1}$$

Assuming that each averaged variable, x, can be represented as: $x = X + \hat{x}$, where X is the value of the variable at the operation point (either a constant value or a value with 50Hz periodic variation), and $\hat{x}$ is the small-signal variation around the operation point, equation (1) can be rewritten as (2), where, D is the duty cycle at the operating point:

$$V_o + \hat{v}_o = (V_{DC} + \hat{v}_{DC}) \cdot \left(2 \cdot \left(D + \hat{d}\right) - 1\right) \tag{2}$$

Separating the operation point (OP) values and the small-signal terms it is obtained:

$$V_o = V_{DC} \cdot (2 \cdot D - 1) \tag{3}$$

$$\hat{v}_o = \hat{v}_{DC} \cdot (2 \cdot D - 1) + 2 \cdot V_{DC} \cdot \hat{d} \tag{4}$$

Similarly, the OP and small-signal terms can be obtained for the relationship between the input and the output current.

$$I_i = I_L \cdot (2 \cdot D - 1) \tag{5}$$

$$\hat{\imath}_i = \hat{\imath}_L \cdot (2 \cdot D - 1) + 2 \cdot I_L \cdot \hat{d} \tag{6}$$

Fig. 2, shows the equivalent model of the inverter around the operation point. In this model the averaged variables D'(t)=2·D-1, IL(t) and Vo(t) undergo a slow (50Hz) variation in terms of the switching frequency. Indeed, the operation point is varying at 50Hz. Equations (7) and (8) show the expressions of the inductor current I_L and the duty cycle D at the operation point. A resistive load has been considered, $Z_{load} = R$, but a general transfer function for the load impedance $Z_{load}(s)$ could be used.

$$I_L = \frac{\sqrt{2}\cdot V_{o_{RMS}}}{R} \cdot \cos(\omega t) + \frac{\sqrt{2}\cdot V_{o_{RMS}}}{|Z_C|} \cdot \cos(\omega t - \phi_C) \tag{7}$$

$$D = \frac{1}{2} + \frac{V_{o\_RMS}}{\sqrt{2}\cdot V_{DC}} \cdot \left(-\frac{\omega L}{R} \cdot \mathrm{sen}(\omega t) - \frac{\omega L}{|Z_C|} \cdot \mathrm{sen}(\omega t - \phi_C) + \cos(\omega t) \right) \tag{8}$$

In (7) and (8) the following expressions are used: $|Z_C| = \sqrt{(R_d)^2 + (1/\omega \cdot C)^2}$, $\phi = atan(-1/\omega \cdot C \cdot R_d)$ and $\omega = 2\pi \cdot 50$ rad/s.

From equations (4) and (6) it is possible to obtain the small-signal model of the inverter shown in Fig. 3.

A usual way to control the inverter output voltage is by means of two cascaded loops: an internal current loop on $\hat{\imath}_L$ and an external voltage loop on $\hat{v}_O$, as it is shown in Fig. 4. In Fig. 4, $G_s(s)$ represents the current control loop controller and $RD(s)$ is the transfer function of a digital delay of one switching period (a digital implementation is assumed) defined as:

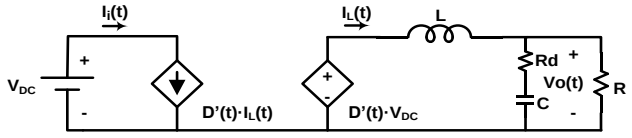

Fig. 2. Equivalent averaged model of the inverter around the operation point.

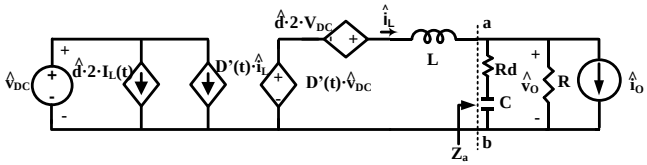

Fig. 3. Inverter small-signal model.

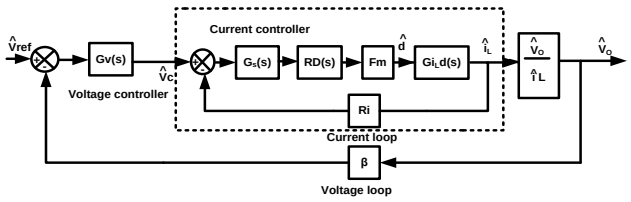

Fig. 4. Cascaded control loop of the inverter in island mode operation

$$RD(s) = \frac{1-\left(\frac{s*T_s}{2}\right)+\left(\frac{(s*T_s)^2}{12}\right)}{1+\left(\frac{s*T_s}{2}\right)+\left(\frac{(s*T_s)^2}{12}\right)} \quad (9)$$

Where, T_s is the switching period ($T_s = 50\mu s$), $R_i = 0.2\ \Omega$ is the current sensor gain, $\beta = 0.006$ is the output voltage sensor gain and F_m is the gain of the bipolar PWM modulator, given by (10).

$$F_m = \frac{1}{V_{pp-Triangular}} = 1 \quad (10)$$

The transfer function of interest for the design of the current loop is that from the duty cycle to the output current, $G_{iL-d}(s)$ expressed by (11).

$$G_{iL\_d}(s) = \frac{\hat{i}_L}{\hat{d}}\Big|_{\hat{v}_{DC}=0} = \frac{2 \cdot V_{DC}}{Z_a + s \cdot L} \quad (11)$$

Where Z_a, is the load impedance in parallel with the output capacitor (12), and V_{DC} is the DC_Link voltage.

$$Z_a = \left(R_d + \frac{1}{sC}\right) \| R = \frac{(s \cdot C \cdot R_d + 1) \cdot R}{s \cdot C(R_d + R) + 1} \quad (12)$$

IV. Current Controller Design.

For the current loop a P + Resonant controller [12] with the following transfer function has been chosen:

$$G_S(s) = K_P + \frac{K_1 \cdot B_1 \cdot s}{s^2 + B_1 \cdot s + (\omega_1^2)} \quad (13)$$

The proportional gain K_P can be determined by (14), where $\omega_{Ci}\_desired$ is the desired crossover angular frequency of the current loop. In this case it is chosen: $\omega_{Ci}\_desired = 2 \cdot \pi \cdot 1800$ *rad/s.*

$$K_P = \frac{L \cdot \omega_{Ci\_desired}}{R_i \cdot F_m \cdot 2 * V_{DC}} = 1.34 \quad (14)$$

For this application the following parameters have been chosen: $k_1 = 100, B_1 = 2\pi\ rad, \omega_1 = 2 * \pi * 50\ rad/s$. The implementation of this controller produces a current loop with the following stability characteristics: f_{Ci} = 2.21 kHz (gain crossover frequency), PM=64.5º (Phase Margin), GM=8.51 dB (Gain Margin). The Bode plot of the loop gain of the current loop, $T_i(s)$, is depicted in Fig. 5.

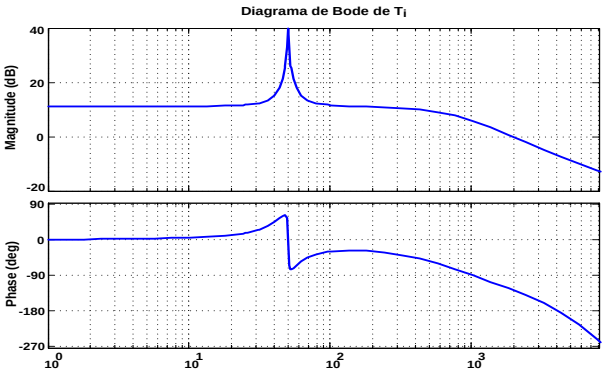

Fig. 5. Bode plots of the current loop.

V. Voltage Regulator Design

A. Conventional PI voltage controller

For comparison purposes a simple PI [13] controller and PI + Resonant controller have been chosen. The design is based on the block diagrams of Fig. 4 and Fig. 5, where GV(s) is a PI controller and $G_{vres}(s)$ is a PI + Resonant controller. The expression of the PI controller is given by (15).

$$Gv(s) = 0.32605 \cdot \frac{s+4.21e3}{s} \quad (15)$$

The loop gain, $T_V(s)$, of the voltage loop can be obtained as (16), where $G_{vo\_vc}(s) = v_o(s)/v_c(s)$ is the closed loop transfer function of the current loop. The term β is the gain of the inverter output voltage sensor, β=0.006.

$$T_V(s) = Gv(s) \cdot G_{vo\_vc}(s) \cdot \beta \quad (16)$$

The voltage loop with the PI controller has the following stability characteristics: f_{Cv} = 815 Hz (gain crossover frequency), PM=103º (Phase Margin) and GM=6.53 dB (Gain Margin).

B. PI + Resonant voltage controller

A usual method for improving the tracking of the inverter output voltage reference is to use a PI + Resonant voltage controller [12-13]. The same P + Resonant current controller as in section 4. A is used, described by (13) and (14). The resulting control block diagram is shown in Fig. 6. The voltage is controller aims both to improve the reference tracking and to reduce the inverter output impedance at the fundamental frequency of the output voltage and its odd harmonics, up to the seventh harmonic in this case. The transfer function of the voltage controller is shown by (17).

$$Gv_{res(s)} = C(s) + \sum_{h=1}^{7} \frac{K_h * B_h * s}{s^2 + B_h * s + (\omega_h^2)}, h = odd \quad (17)$$

In (17), C(s) is a proportional controller with a high frequency real pole, designed to perform with the adequate gain and phase margins. In this case C(s) = 5472*(1/s+11000).

The rest of the resonant controller parameters values are shown in Table 2. The loop gain, $T_v(s)res$, of the voltage loop can be described by (18).

$$T_V(s)_{res} = Gv_{res}(s) \cdot G_{vo\_vc}(s) \cdot \beta \quad (18)$$

The voltage loop with the P + resonant controller has the following stability characteristics: f_{Cv} = 920 Hz (gain crossover frequency), PM=86.7º (Phase Margin) and GM=6.87 dB (Gain Margin).

C. Two degrees of freedom voltage control with repetitive controller (R2DOF)

In the proposed control the previously described P + Resonant current controller (13) (14) is used, but the voltage controller is based on a two degrees of freedom control (2DOF) [14-15] combined with a Repetitive Controller [16-17]. The 2DOF control technique can correct disturbances in the system and it has a good response to changes in the reference signal.

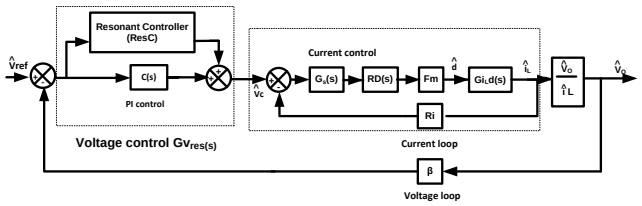

Fig. 6. Cascaded control loop of the inverter in island mode operation with PI + Resonant voltage controller.

TABLE 2.
RESONANT CONTROLLER PARAMETERS.

Harmonic	Gains		BW	
1	K1	25	B1	2·π·0.5
3	K3	20	B3	2·π·1.5
5	K5	15	B5	2·π·2.5
7	K7	10	B7	2·π·3.5

This technique seeks to process the reference signals and the output independently, resulting in various methods of tuning. 2DOF control is more robust that the One Degree of Freedom technique.

Adding a repetitive controller to the 2DOF control scheme contributes to the improvement of the disturbance rejection at certain frequencies, thus reducing the inverter output THDv. Repetitive control, whose operation is based on the Internal Model Principle (IMP) [18], is capable of tracking periodic references and of rejecting periodic disturbances. The addition of this regulator is seeking to maintain the waveform, amplitude and frequency of the output signal.

The design of the proposed control is based on the scheme of Fig.7, where it is only shown the voltage loop. The inner current loop is closed. In Fig. 7 the block RC(s) depicts the repetitive controller, C1(s) is a proportional controller more real pole and C2(s) is a P controller. It is possible to deduce the following transfer functions, where $\hat{p}(s)$ represents any disturbance of the output voltage:

$$\boldsymbol{G_{vo\_vref}(s)} = \frac{\hat{v}_o}{\hat{v}_{ref}}\Big|_{\hat{p}(s)=0} = \frac{G_{vo\_vc}\cdot C1(s)+RC(s)}{1+[C1(s)+RC(s)+C2(s)]\cdot G_{vo\_vc}*\beta} \quad (19)$$

$$\boldsymbol{G_{vo\_p}(s)} = \frac{\hat{v}_O(s)}{\hat{p}(s)}\Big|_{\hat{v}_{ref}=0} = \frac{1}{1+(C1(s)+RC(s)+C2(s))\cdot G_{vo\_vc}*\beta} \quad (20)$$

The goal of the R2DOF control is to meet the following conditions:

$$\boldsymbol{G_{vo\_vref}(s)} = \frac{\hat{v}_o(s)}{\hat{v}_{ref}(s)} \approx \frac{1}{\beta} \quad (21)$$

$$\boldsymbol{G_{vo\_p}(s)} = \frac{\hat{v}_O(s)}{\hat{p}(s)} \to 0 \quad (22)$$

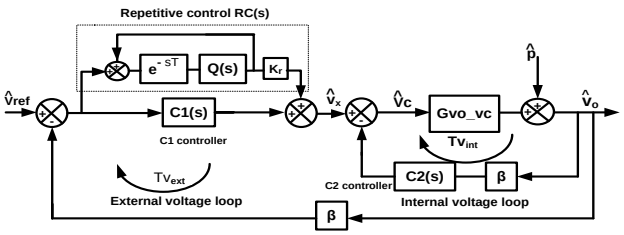

Fig. 7. Block diagram of the voltage loop with R2DOF Control. The current loop is closed.

The chosen regulators have the following values:

$$C2(s) = 0.15 \quad (23)$$

$$C1(s) = 3860 \cdot \frac{1}{s+7000} \quad (24)$$

$$\boldsymbol{RC(s)} = \frac{\boldsymbol{Q(s)}\cdot e^{-sT}}{\boldsymbol{1-Q(s)}\cdot e^{-sT}} * \boldsymbol{Kr} \quad (25)$$

$$\boldsymbol{Q(s)} = \frac{1}{\frac{s^2}{\omega_q^2}+\frac{2\varepsilon}{\omega_q}s+1} \quad (26)$$

In (25) and (26), Q(s) represents a second order infinite impulse response (IIR) low pass filter. The term $\omega_q = 2 * \pi * f_q$ (rad/seg) is the cutoff frequency of the IIR filter with f_q= 400Hz and a damping factor: $\varepsilon = 0.707$. The transfer function e^{-sT} represents a delay of one period of the load voltage fundamental frequency (T = 0.02 s), and $Kr = 0.5$ is the gain of the repetitive controller.

The values of fq and Kr are chosen to maintain adequate stability margins. Applying block algebra to Fig. 7, the loop gain of the 2DOF voltage loop with repetitive controller (R2DOF) can be derived, following (27).

$$Tv_{ext}(s) = [C1(s) + RC(s) + C2(s)] \cdot G_{vo\_vc} \cdot \beta \quad (27)$$

The voltage loop gain with R2DOF exhibits the following stability characteristics: f_{Cv}=954 Hz (gain crossover frequency), PM=102º (Phase Margin) and GM=8.21 dB (Gain Margin).

Fig.8 shows the Bode plots of the voltage loop gain with the three voltage controllers (PI, PI + Resonant and R2DOF) previously described. It is observed that the PI + Resonant and R2DOF controls present a high gain of the voltage loop gain at the fundamental of the output voltage and at its odd harmonics.

This behavior ensures both a good reference tracking and a high disturbance rejection at those frequencies. The same cannot be affirmed for the PI controller.

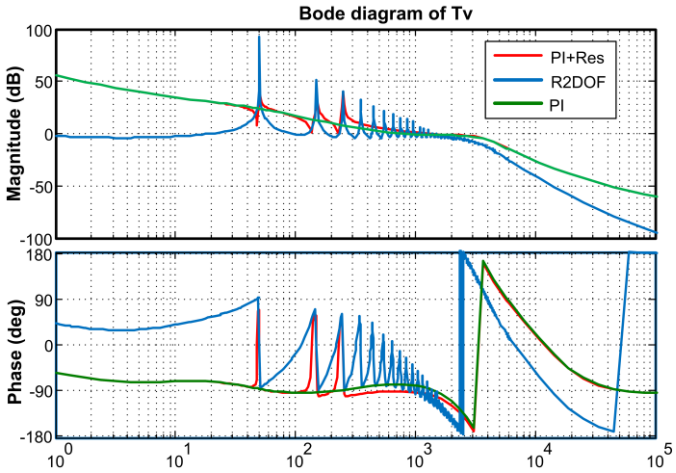

Fig. 8. Bode plots of the voltage loop gain: PI and PI + Resonant voltage controller vs. R2DOF voltage control.

Fig. 9 depicts the Bode plots of the closed loop voltage reference following transfer function (19), $G_{vo\_vref}(s)$, with PI, PI + Resonant and R2DOF voltage control. It is observed a null error in the reference tracking at the fundamental of the output voltage and of its lower odd harmonics (up to the 7TH) in the case of PI + Resonant and R2DOF voltage controllers.

Note that at those frequencies the phase of $G_{vo\_vref}(j\omega)$ is close to 0º for the PI + Resonant and R2DOF controllers, whereas it is observed a negative phase with the PI controller.

VI. Inverter Output Impedance

In order to illustrate the advantages of R2DOF voltage control, the inverter closed-loop output impedance is calculated. First, the inverter open-loop output impedance, $Z_{O\_OL}(s)$, must be deduced. This is done by analyzing the small-signal model of Fig. 3 and the control scheme of Fig. 4.

The transfer function $Z_{O\_OL}(s)$ is calculated assuming $\hat{v}_{DC} = \hat{v}_C = 0$ and a constant voltage at the DC_Link.

$Z_a(s)$, expressed by (28), is the impedance connected to the right side of the filter inductor (see Fig. 3).

$$Za(s) = \frac{R\cdot(s\cdot C\cdot R_d+1)}{s\cdot C\cdot(R_d+R)+1} \tag{28}$$

Applying Kirchhoff laws to the small-signal model of Fig. 3, and taking into account that $\hat{v}_{DC} = 0$ the following equations are derived:

$$Z_{O\_OL} = \frac{\hat{v}_o}{\hat{i}_o} \tag{29}$$

where $\hat{i}_o$ represents a disturbance in the inverter output current (see Fig. 3). When the voltage loop is open ($\hat{v}_C = 0$), (30) can be derived from Fig. 4.

$$\hat{d} = K(s)\cdot \hat{i}_L \tag{30}$$

Where, $K(s) = -Fm\cdot Ri\cdot Gs(s)\cdot RD(s)$.

$$\hat{v}_O = (\hat{i}_L - \hat{i}_O)\cdot Z_a \tag{31}$$

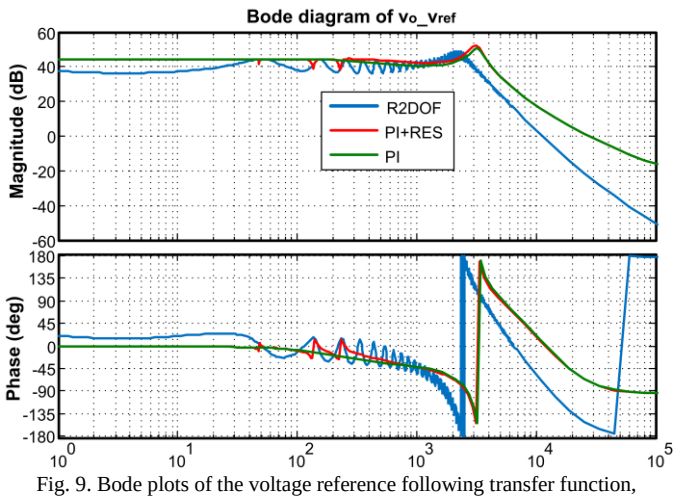

Fig. 9. Bode plots of the voltage reference following transfer function, Gvo_vref(s): PI and PI + Resonant voltage controller vs. R2DOF voltage control.

Considering:

$$2V_{dc}\cdot K(s)\cdot \hat{i}_L = s\cdot L\cdot \hat{i}_L + \hat{v}_o \tag{32}$$

Solving $\hat{i}_L$ from (32) results in (33)

$$\hat{i}_L = \frac{\hat{v}_O}{2V_{dc}\cdot K(s)-s\cdot L} \tag{33}$$

Substituting (33) in (31) results in (34)

$$\hat{v}_o = \left(\frac{\hat{v}_o}{2V_{dc}\cdot K(s)-s\cdot L} - \hat{i}_O\right)\cdot Z_a \tag{34}$$

(35) is obtained from (34)

$$\hat{v}_o\cdot\left(1-\frac{Z_a}{2V_{dc}\cdot K(s)-s\cdot L}\right) = -\hat{i}_O\cdot Z_a \tag{35}$$

Finally, from (35) it is obtained the inverter open loop output impedance, expressed by (36):

$$Z_{O\_OL} = \frac{\hat{v}_o}{\hat{i}_o}\bigg|_{\hat{v}_C=0} = \frac{-Z_a(2V_{dc}\cdot K(s)-s\cdot L)}{2V_{dc}\cdot K(s)-s\cdot L-Z_a} \tag{36}$$

The inverter closed loop output impedance is given by (37), where $T_V(s)$ is given by (16) in the case of a conventional PI voltage controller, by (18) ($T_v(s)$res) in the case of a PI + Resonant controller, or by (27) ($T_V$ext(s)) in the case of a R2DOF controller.

$$Z_{O-CL}(s) = \frac{\hat{v}_o}{\hat{i}_o}\bigg|_{\hat{v}_{DC}=\hat{v}_{Ref}=0} = \frac{Z_{O-OL}(s)}{1+T_V(s)} \tag{37}$$

Fig. 10. shows the Bode plots of the inverter closed-loop output impedance with PI, PI + Resonant voltage controller and R2DOF voltage control. If the voltage controller is a PI one, $Z_{O\text{-}CL}(j\omega)$ has an inductive behavior at low frequency.

In the case of PI + Resonant and R2DOF voltage control, $|Z_{O\text{-}CL}|$ exhibits a very low value at the fundamental of the output voltage and of its odd harmonics. Note that odd current harmonics are generated by nonlinear loads like rectifiers. Besides, it is observed a 0º phase of $Z_{O\text{-}CL}(j\omega)$ at these frequencies, i.e. the inverter output impedance is resistive at the frequency components of the load current.

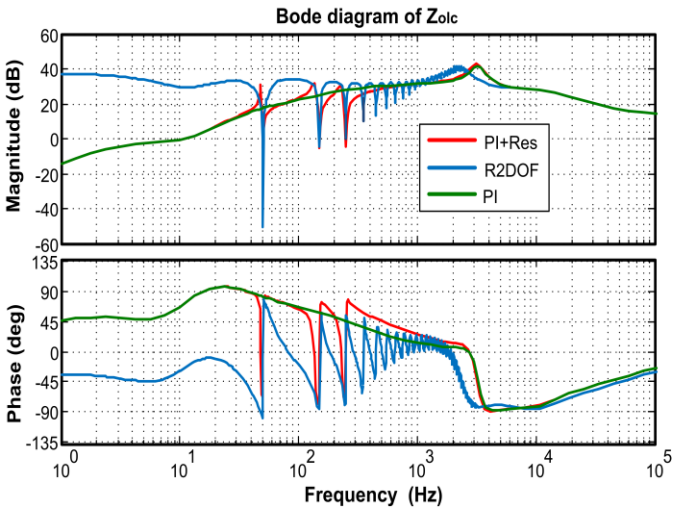

Fig.10. Bode plots of Z_{O-CL} with PI and PI+Resonant voltage controller vs. R2DOF voltage control

The results justify the application of PI + Resonant and R2DOF control. As it will be shown in the following, PI + Resonant and R2DOF voltage control exhibits a better load disturbance rejection than the PI controller, reducing the distortion of the inverter output voltage, especially when nonlinear loads are connected.

VII. SIMULATION RESULTS

Simulations were conducted by means of PSIM™ software.

Fig. 11 shows the voltage and current at the inverter output with R2DOF voltage control, feeding a 315W resistive load (170Ω) at an inverter output voltage of 230VRMS. It is possible to observe a good performance of this controller with a THDv = 0.5 %. The results with PI and P + Resonant controllers feeding the same load are similar, exhibiting a THDv value of 0.9 % and 0.7 %, respectively.

Fig. 12 shows the inverter output voltage and current, respectively, with PI voltage controller feeding a nonlinear load composed by a single phase diode bridge rectifier with a filter capacitance of $C_f = 90\mu F$ in parallel to a 680Ω resistance. The crest factor of this load is CF=4.2 and the apparent power is S=130 VA when connected to an ideal 230 VRMS voltage source. A low performance is observed, with a THDv = 9.2 %. Note that IEEE Standard 519-1992 allows a maximum THDv of 5%. This Standard establishes limits for harmonic voltages on the utility transmission and distribution system, as well as for harmonic currents within industrial distribution systems.

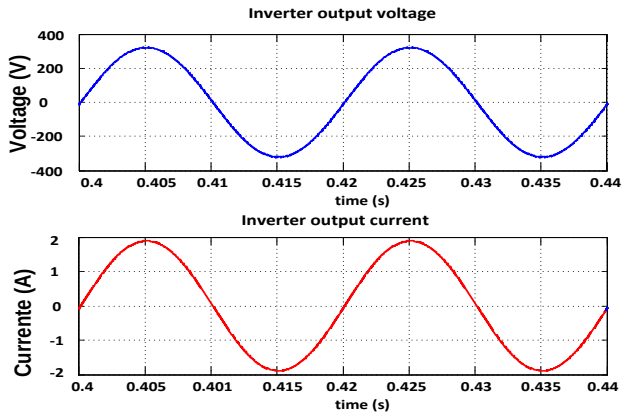

Fig. 11. Voltage and current at the inverter output with a R2DOF control.

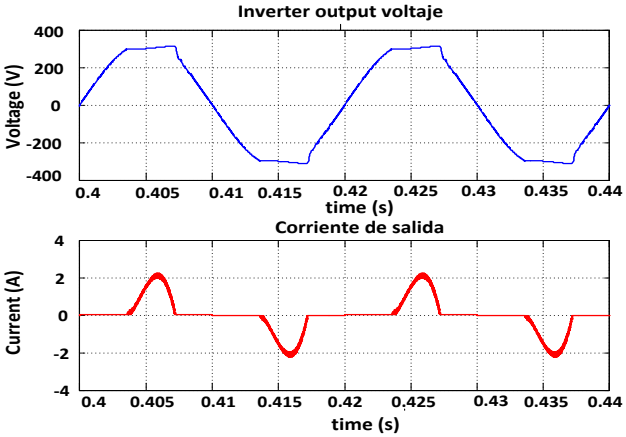

Fig. 12. Voltage and current at the inverter output with nonlinear load, PI controller.

Fig. 13 shows the inverter output voltage and current, respectively, with PI + Resonant voltage controller feeding the previously described nonlinear load. It exhibits a THDv = 5.2 %.

Fig. 14. shows the voltage and current at the inverter output with R2DOF voltage control, feeding the previously described nonlinear load. It presents a good performance, obtaining a THDv = 2.2 %.

Fig. 15 shows the comparative harmonics contents of the inverter output voltage supplying the previously defined nonlinear load with both controllers. R2DOF control reduces the THDv from 9.2 % (PI) and 5.2 % (PI + Resonant) to 2.2 %.

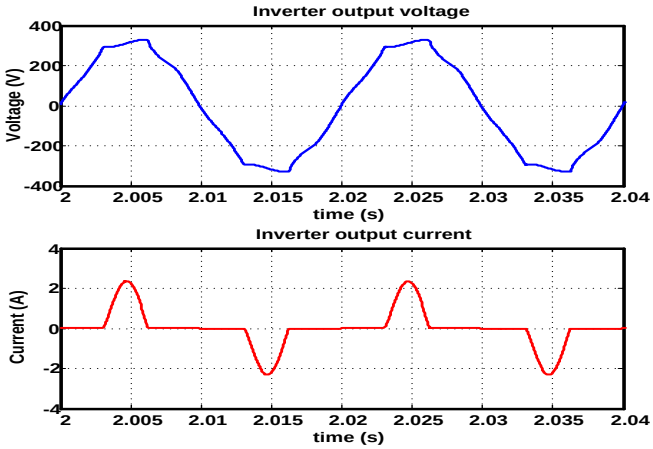

Fig. 13. Voltage and current at the inverter output with nonlinear load, PI + Resonant controller

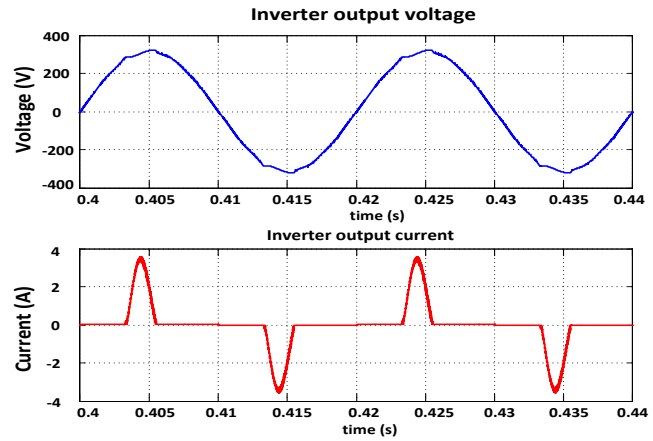

Fig. 14. Voltage and current at the inverter output with. nonlinear load, R2DOF control.

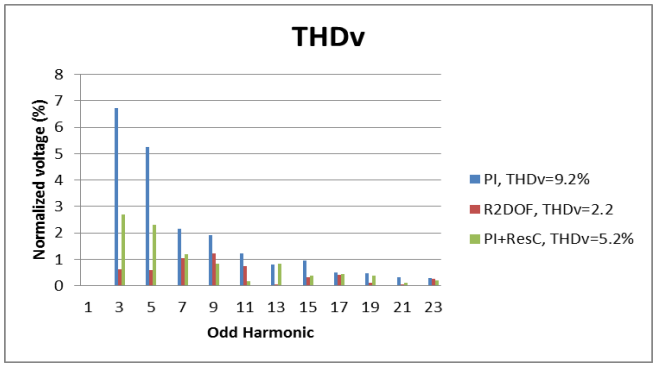

Fig. 15. R2DOF control vs. conventional PI and P + Resonant controller. Harmonics of the inverter output voltage supplying a nonlinear load.

VIII. CONCLUSIONS

In this paper it is presented the design, implementation, simulation and experimental results of an innovative Repetitive Two-Degrees of Freedom (R2DOF) control scheme applied to the output voltage loop of grid-isolated single-phase inverters working in a microgrid. This scheme combines the disturbance rejection properties of two control techniques: repetitive and 2-degrees of freedom control. Simulation and experimental results show that the proposed control scheme can effectively reduce the output voltage distortion produced by the current harmonics produced by strongly nonlinear loads. The THDv at inverter output for a nonlinear load with a crest factor of CF=4.2 is reduced from 9.2% with a PI controller and 5.2 % with a PI + Resonant controller to 2.2% with R2DOF control. The proposed control widely fulfills the IEEE 519-1992 norm.

ACKNOWLEDGMENT

The first author thanks the support of the Instituto Politécnico Nacional (IPN), of the Comisión de Operación y Fomento de Actividades Académicas (COFAA).

REFERENCES

[1] Zhixin Miao; Domijan, A.; Lingling Fan; "Investigation of Microgrids With Both Inverter Interfaced and Direct AC-Connected Distributed Energy Resources," Power Delivery, IEEE Transactions on , vol.26, no.3, pp.1634-1642, July 2011.

[2] Patel, H.; Agarwal, V.; , "Control of a Stand-Alone Inverter-Based Distributed Generation Source for Voltage Regulation and Harmonic Compensation," Power Delivery, IEEE Transactions on , vol.23, no.2, pp.1113-1120, April 2008.

[3] C.L. Trujillo, D. Velasco, E. Figueres, G. Garcerá. Analysis of active islanding detection methods for grid-connected microinverters for renewable energy processing Original Research Article Applied Energy, Volume 87, Issue 11, November 2010,.Pages-3591-3605

[4] IEEE STD. 519-1992, IEEE Recommended Practices and Requirements for Harmonic Control in Electric Power Systems, IEEE Industry Applications Society/Power Engineering Society.

[5] H.L. Broberg, R.G. Molyet. Reduction of repetitive errors in tracking of periodic signals: theory and application of repetitive control, Control Applications, First IEEE Conference on, Volume 2, 13-16 Sep 1992, pp.1116-1121

[6] M. Araki and H. Taguchi, Tutorial Paper Two-Degree-of-Freedom PID Controllers, Automation, and Systems Volume 1, No. 4, December 2003.

[7] A. Emadi, A. Ñasiri, and S.B. Bekiaarov, Uninterruptible Power Supplies and Active Filters, Boca Raton: CRC Press, 2005.

[8] PSIM 7.0,. Users Guide (2006), Powersim Inc.

[9] Crebier, J.C.; Ferrieux, J.P., "PFC full bridge rectifiers EMI modelling and analysis common mode disturbance reduction," Power Electronics, IEEE Transactions on , Volume.19,no.2, pp. 378-387, March 2004.

[10] Vorperian, V., "Simplified analysis of PWM converters using model of PWM switch. Continuous conduction mode," Aerospace and Electronic Systems, IEEE Transactions on., Volume.26, no.3, pp.490- 496, May 1990.

[11] N. Mohan, T.M. Underland., W.P. Robbins. Power electronics: converters, applications, and design, 3th ed. John Wiley & Sons, 2003.

[12] D.N. Zmood, D.G. Holmes., "Stationary frame current regulation of PWM inverters with zero steady-state error.," Power Electronics, IEEE Transactions on, vol.18, no.3, pp. 814-822, May 2003.

[13] Kuo, B.C.; Golnaraghi, F., "Automatic control systems, "John Wiley & Sons, 2002.

[14] Miklosovic, R.; Gao, Z., "A robust two-degree-of-freedom control design technique and its practical application," Industry Applications Conference, 2004. 39th IAS Annual Meeting., Conference Record of the 2004 IEEE , Volume.3, no., pp. 1495- 1502 vol.3, 3-7 Oct. 2004.

[15] Zhao Qinglin; Guo Xiaoqiang; Wu Weiyang; , "Two-degree-of-freedom PID digital control of a bidirectional quasi-single-stage push-pull forward high frequency link inverter," Applied Power Electronics Conference and Exposition, 2006. APEC '06. Twenty-First Annual IEEE ,Volume., no., pp. 6 pp., 19-23 March 2006

[16] S. Chen, Y.M. Lai, S. Tan, C.K. Tse. Analysis and design of repetitive controller for harmonic elimination in PWM voltage source inverter systems. Power Electronics, IET, Volume 1, no.4, pp. 497-506, 2008.

[17] S. Chen,, Y.M. Lai, S.C. Tan, C.K. Tse, Optimal design of repetitive controller for harmonic elimination in PWM voltage source inverters, Telecommunications Energy Conference, 2007. INTELEC 2007., 29th International, Volume, no, Sept. 30 2007-Oct. 4 2007, pp.236-241.

[18] B.A. Francis and W.M. Wonham. The internal model principle of control theory., Automatica., Volume 12, Issue 5, September 1976, pp. 457-465.

Rubén Ortega received the B.Sc. degree in electrical engineering in 1999 and the M.Sc. degree in systems engineering from the Instituto Politécnico Nacional, Mexico, Mexico, and the D.E.A. degree in electrical engineering, computer, and electronic system from the Universidad de Oviedo, Oviedo, Spain, in 2009. He is currently working toward the Ph.D. degree at the Universidad Politécnica de Valencia, Valencia, Spain. He is also currently a Professor with the Department of Computer Science and Engineering, Escuela Superior de Cómputo, Instituto Politécnico Nacional. His main research fields are in modeling and control of power converters applied to the distributed generation in microgrids.digital signal processing.

Oscar Carranza received the B.S. degree in Communication and Electronics Engineering from the Instituto Politecnico Nacional, Mexico City, Mexico, in 1996, the M.Sc. degree in Electronics Engineering from the Instituto Politecnico Nacional, Mexico City, Mexico, in 1999, and the Ph.D. degree in Electronics Engineering from the Universidad Politécnica de Valencia, Valencia, Spain, in 2012. He has been professor in Escuela Superior de Computo, Instituto Politecnico Nacional since 1999. His main research fields are in modeling and control of power converters, power processing of renewable energy sources, and grid-connected converters for distributed power.

César L. Trujillo received the B.S. degreein electronics engineering from the Universidad Distrital Francisco José de Caldas, Bogotá, Colombia, in 2003, the M.Sc. degree in electrical engineering from the Universidad Nacional de Colombia, Bogotá, in 2006, and the Ph.D. degree in electronics engineering from the Universidad Politécnica de Valencia, Valencia, Spain, in 2011. He is an Associate Professor with the Department of Electronic Engineering, Universidad Distrital Francisco José de Caldas. He is also currently with the Grupo de Sistemas Electrónicos Industriales, Departamento de Ingeniería Electrónica, Universidad Politécnica de Valencia. His main research interests include modeling and control of power converters applied to the distributed generation in microgrids.

Julio C. Sosa received the B.S. degree in Electronic Engineering in 1997 from Instituto Tecnológico de Lazaro, Mich. Mexico. The M. Sc in Electrical Engineering, in 2000 from CINVESTAV-IPN, Mexico and the PhD in Technology of Information and Computation in 2007 fron the University of Valencia, Spain. He is profesor of computer architecture at Escuela Superior de Computo, Instituto Politecnico Nacional, Mexico D. F. since 1997. His current research interests are reconfigurable systems, digital signal processing and embedded systems.